Cross sections and tensor analyzing powers A_{yy} of the reaction $^1H(\vec{d},pp)n$ in "symmetric constant relative energy" geometries at $E_d = 19$ MeV

J. Ley, C. Düweke, R. Emmerich, A. Imig, and H. Paetz gen. Schieck*
Institut für Kernphysik, Universität zu Köln, Zülpicher Straße 77, D-50937 Köln, Germany

J. Golak and H. Witała
Institute of Physics, Jagiellonian University, Reymonta 4, PL-30059 Cracow, Poland

E. Epelbaum
Jefferson Laboratory, Theory Division, Newport News, Virginia 23606, USA

A. Deltuva and A. C. Fonseca
Centro de Física Nuclear da Universidade de Lisboa, P-1649-003, Lisboa, Portugal

W. Glöckle
Institut für Theoretische Physik, Ruhr-Universität Bochum, Universitätsstraße 150, D-44780 Bochum, Germany

U.-G. Meißner
Helmholtz-Institut für Strahlen- und Kernphysik (Theorie), Universität Bonn, Nussallee 14-16, D-53115 Bonn, Germany, and Institut für Kernphysik, Forschungszentrum Jülich, D-52425 Jülich, Germany

A. Nogga
Institut für Kernphysik, Forschungszentrum Jülich, D-52425 Jülich, Germany

P. U. Sauer
Institut für Theoretische Physik, Universität Hannover, D-30167 Hannover, Germany
(Received 20 February 2006; published 7 June 2006)

We measured the cross sections and tensor analyzing powers of the $^1H(\vec{d},pp)n$ breakup reaction at $E_d = 19$ MeV in four symmetric constant relative energy (SCRE) configurations. The data are compared with theoretical predictions from four different approaches: the first based on high-precision (semi)phenomenological potentials alone or, the second, combined with model three-nucleon forces, and the third based on chiral forces up to next-to-next-to-leading order (NNLO) in the chiral expansion. In these cases the Coulomb interaction is not included. In addition, a fourth approach consists in a comparison with predictions based on CD Bonn including the Δ excitation and the Coulomb force. In all cases the measured cross sections are significantly below the theoretical values, whereas the magnitudes of the tensor analyzing powers agree within the error bars in three of the four cases. The apparent discrepancies in the breakup cross sections are similar to the known differences for the space-star breakup. This adds to the data base of unsolved low-energy discrepancies (puzzles).

DOI: 10.1103/PhysRevC.73.064001 PACS number(s): 25.10.+s, 25.45.−z, 21.30.−x, 21.45.+v

I. INTRODUCTION

The three-nucleon system has for a long time been the testing ground for nucleon-nucleon forces as they act in the lightest systems composed of nucleons. State of the art calculations—using Faddeev techniques in momentum space—of the three-nucleon scattering allow the comparison of numerically exact theoretical predictions with a wide range of observables such as elastic or breakup cross sections and polarization data. Though the overall agreement between theory and experiment is rather good, there remain certain discrepancies [1]. The most prominent one is the drastic underprediction of the nucleon-deuteron (Nd) vector analyzing power A_y at energies below ≈25 MeV by all modern NN potentials [1]. In both the proton-deuteron (pd) and neutron-deuteron (nd) elastic scattering, the theoretical prediction is about 30% below the data in the angular region of the analyzing power maximum [2–4]. For the same reaction, but for energies above ≈60 MeV, the minima of the differential cross section are also underpredicted if only two-nucleon ($2N$) forces are used [5, 6]. Although this discrepancy can be removed once three-nucleon forces ($3NF$s) are also taken into account, the low-energy A_y problem has not been resolved yet.

For the breakup process the low-energy nd space-star (SST) configuration in which all three nucleons are emerging in the c.m. system with equal magnitudes of momenta in a plane perpendicular to the incoming beam direction still presents

*Corresponding author: Email: schieck@ikp.uni-koeln.de

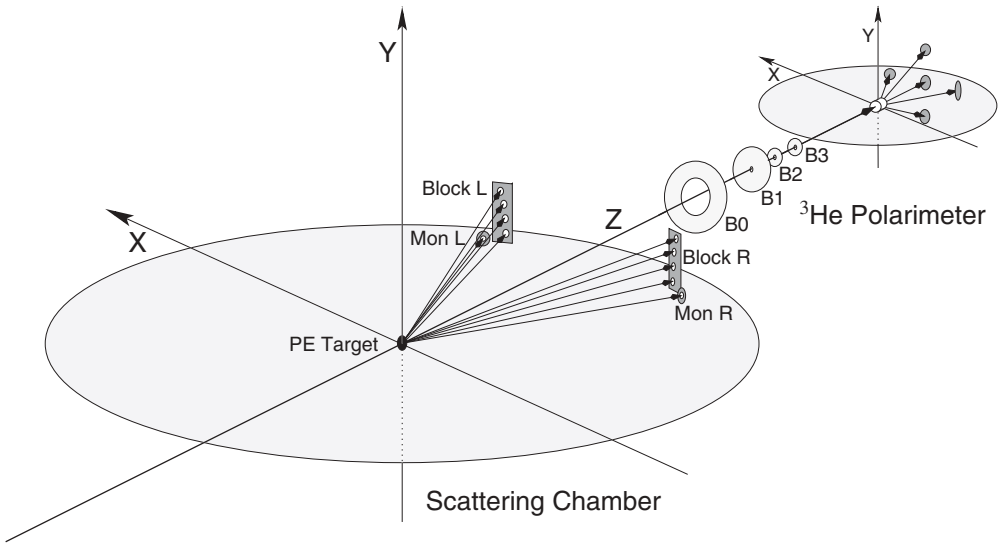

FIG. 1. Schematic of the ORTEC 2800 scattering chamber and the ^{3}He$(d,p)^4$He deuteron vector and tensor polarimeter together with its beam-defining apertures B0 to B3.

a puzzle. Modern NN forces give too small nd space-star cross sections at low energies [7–11]. However, in this energy region the pd breakup data are systematically below the theoretical nd predictions and therefore substantially below the corresponding nd data, thus pointing to the importance of Coulomb effects in this configuration [12–15]. Recent momentum-space calculations of the three-nucleon breakup including the Coulomb interaction have shown, however, that the Coulomb effect is far too small to reproduce the difference between pd and nd space-star data [16].

These discrepancies point to the necessity of including new ingredients in addition to the standard two-body input into the $3N$ continuum calculations, such as $3NF$s. However, present-day $3NF$s show only small effects on the low-energy elastic scattering vector analyzing power [17]. However, adding the 2π-exchange Tucson-Melbourne (TM) $3NF$ [18, 19], adjusted to reproduce the experimental triton binding energy [20], or adding the Δ isobar, mediating an effective $3NF$, fills in the Nd elastic scattering cross-section minima at higher energies [5, 6].

The present work with tensor-polarized deuterons was motivated mainly by discrepancies between theoretical predictions and data found in the observable A_{yy} at incoming deuteron energies 94.5 [21] and 52.1 MeV [22]. Besides, breakup tensor analyzing powers have been measured only rarely and

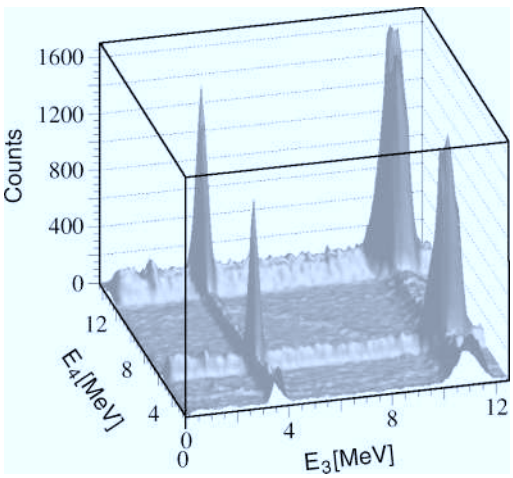

FIG. 2. Calibrated E_3–E_4 energy coincidence matrix for the $\alpha = 56^\circ$ situation before background subtraction. The coincident true events along the kinematical curve are weakly visible.

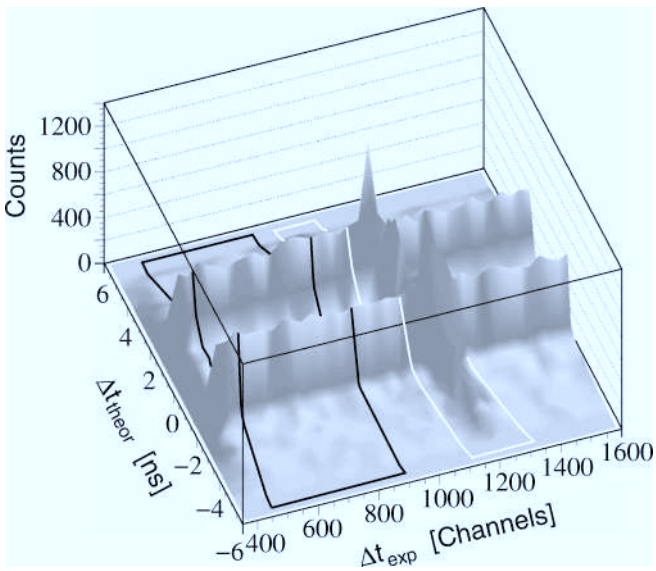

FIG. 3. Time-difference matrix for the $\alpha = 56^\circ$ situation, showing the area of the (true+random) events C(tr+r) marked in white as well as the area of the randomly distributed events C(r) marked in black. The event density is plotted as a function of time-of-flight differences as measured directly, in arbitrary units, and those calculated from measured energies and distances, assuming particle masses to be the nucleon masses. The two horizontal bands are due to coincidences produced by two-particle reactions with random background. For details see, e.g., Ref. [53] and references therein.

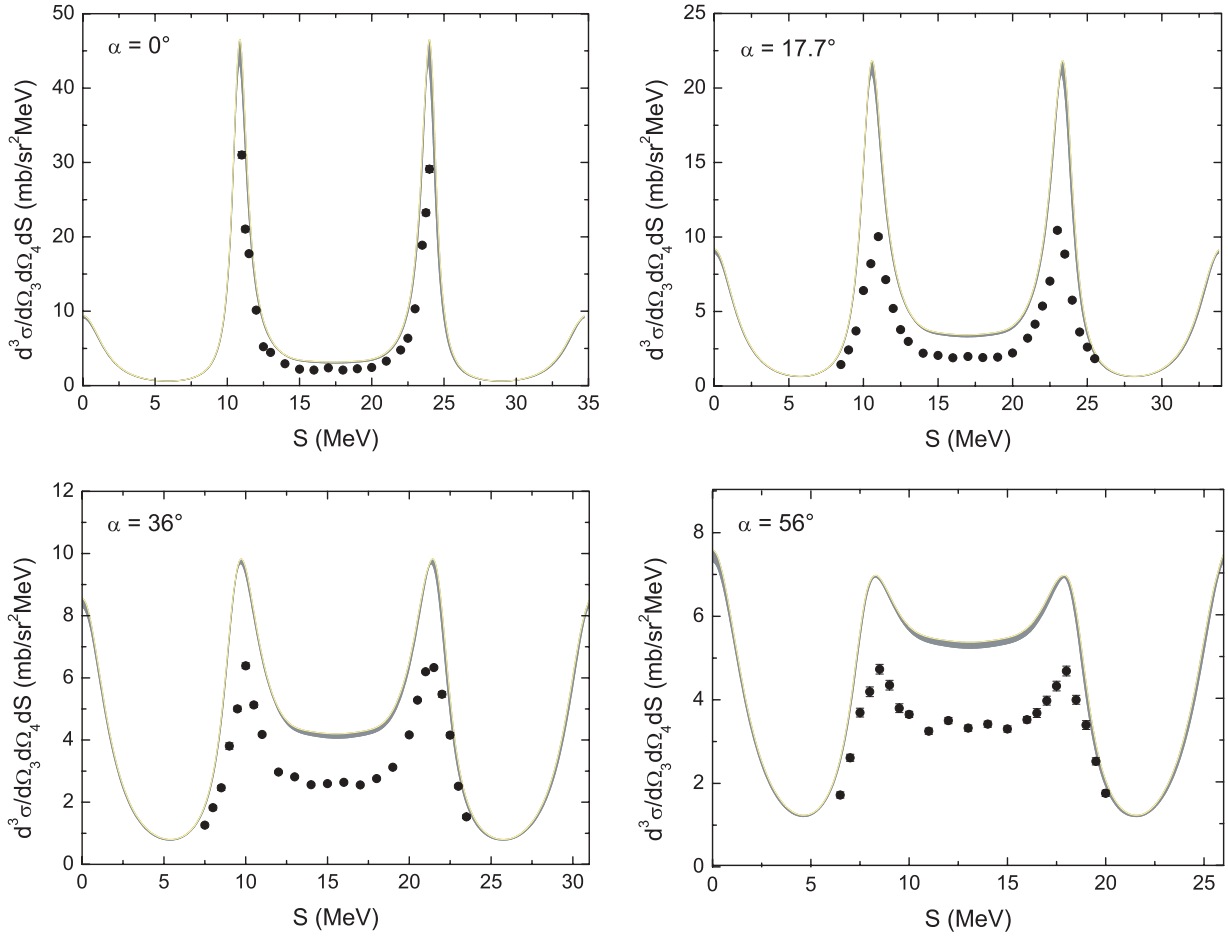

FIG. 4. (Color online) Results of the SCRE breakup cross section $d^3\sigma/d\Omega_3 d\Omega_4 dS$ for $\alpha = 0^\circ, 17.7^\circ, 36.0^\circ, 56.0^\circ$ (see Table I). Experimental data are compared with the results of Faddeev calculations using the Nijmegen1, Nijmegen2, CD Bonn, and AV18 potentials. The gray bands show the range of variation with all four two-body potentials.

therefore are interesting observables. The systematic study of a symmetric constant relative energy (SCRE) geometry, in which the c.m. plane of the space-star configuration is rotated to form some angle with the incoming beam direction, provides noncoplanar breakup situations and thus explores wider areas of the breakup phase space. One of the more classic situations has been the symmetric space star (SST, a special SCRE case) for which good systematic studies exist, at least for cross sections; see e.g. Ref. [23].

In Sec. II we briefly describe the underlying theory. In Secs. III and IV the details of the kinematics, of the experiment, and of the data analysis are given. The resulting data are compared with the theory in Sec. V. We summarize in Sec. VI.

II. THEORY

In this work we present three sets of theoretical predictions. The first set is based on solutions of $3N$ Faddeev equations in momentum space, whereas in the second, besides including the Δ, the Coulomb force is fully taken into account. Finally, predictions by the effective field theory are presented.

A. Classical *nd* approach

In the classical calculations with realistic NN interactions (Argonne AV18 [24], CD Bonn [25], Nijmegen 1 (Nijm1), and Nijmegen 2 (Nijm2) [26]) alone or combined with the Tucson-Melbourne [18, 19] or Urbana IX [27] $3NF$s, the long-range Coulomb force acting between two protons is totally neglected. In the following we give a short overview of the underlying formalism and of the numerical performance. For more detail we refer to Refs. [1, 28–31], and references therein.

The description of the $3N$ scattering is provided by the operator $\tilde{T}$, which sums up all multiple scattering contributions originating from the interactions of three nucleons via $2N$ and $3N$ forces. This operator fulfills the integral equation [31]

$$\tilde{T} = tP + (1 + tG_0)V_4^{(1)}(1 + P) + tPG_0\tilde{T} + (1 + tG_0)V_4^{(1)}(1 + P)G_0\tilde{T}. \quad (1)$$

Here t is the NN t matrix, G_0 is the free $3N$ propagator, and P is the sum of a cyclical and anticyclical permutations of three nucleons. The $3NF$ is split into three parts,

$$V_4 = \sum_{i=1}^{3} V_4^{(i)}, \quad (2)$$

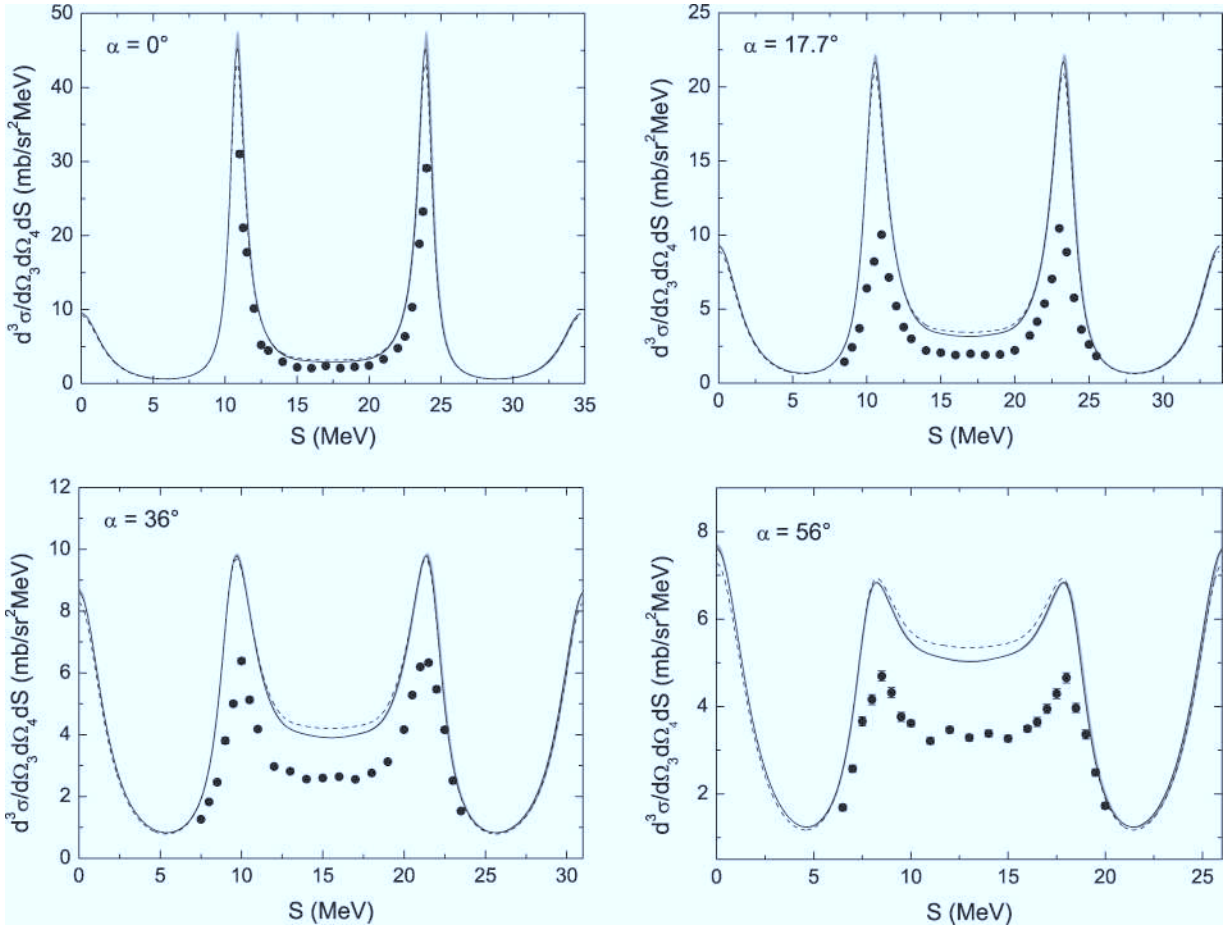

FIG. 5. Results of the SCRE breakup cross section $d^3\sigma/d\Omega_3 d\Omega_4 dS$ for $\alpha = 0^\circ, 17.7^\circ, 36.0^\circ, 56.0^\circ$. Experimental data are compared with the results of Faddeev calculations using the Nijmegen1, Nijmegen2, CD Bonn, and AV18 potentials including the TM99' $3NF$, and, in addition, AV18 with the Urbana IX $3NF$ (black curves) and AV18 without $3NF$ for comparison (dashed curves). The barely discernible gray bands show the overall variation of the results with all four two-body potentials including the TM99' $3NF$ and signify their very close agreement.

where each one is symmetrical under the exchange of two particles. For instance, in the case of π–π exchange $3NF$ [18, 19], such a decomposition corresponds to the three possible choices of the nucleon undergoing off-shell π–N scattering.

The transition operator for the breakup process U_0 can be expressed in terms of a $\tilde{T}$ operator as [1, 31]

$$U_0 = (1 + P)\tilde{T}. \tag{3}$$

We solved Eq. (1) in a partial-wave projected momentum-space basis at the nucleon laboratory energy $E_N^{\rm lab} = 9.5$ MeV by using the AV18, CD Bonn, Nijm1, and Nijm2 potentials. These interactions reproduce the NN data set with high accuracy as measured by a χ^2/datum ratio very close to 1. In the calculations all partial-wave states with total angular momenta in the two-nucleon subsystem up to $j_{\rm max} = 5$ were taken into account. In the state $^1S_0$ the neutron-proton force component has been used. For other isospin $t = 1$ states the charge-independence breaking (CIB) of the NN interaction was taken into account by the 2/3 - 1/3 rule [32].

To check the magnitude of $3NF$ effects we combined the NN potentials with the updated version of the TM $3NF$ (TM99') [33, 34], adjusting its cutoff for a particular NN potential to match the value of the ^{3}H binding energy [20] (in units of the pion mass m_π, cutoff values are 4.764, 4.469, 4.690, and 4.704 for AV18, CD Bonn, Nijm1, and Nijm2, respectively). In addition, the AV18 potential was also combined with the Urbana IX $3NF$ [27].

B. Effects of Δ-isobar excitation and Coulomb force

Another set of theoretical predictions is based on a realistic coupled-channel potential CD Bonn + Δ [35], allowing for a single virtual Δ-isobar excitation and thereby yielding an effective $3NF$ consistent with the two-nucleon force and including exchanges of π, ρ, ω, and σ mesons. The Coulomb interaction between charged baryons is fully included by using screening and the renormalization approach; CIB in the nuclear force is fully taken into account as well. For three particles interacting via hadronic and screened Coulomb potentials we solve the symmetrized Alt-Grassberger-Sandhas equations

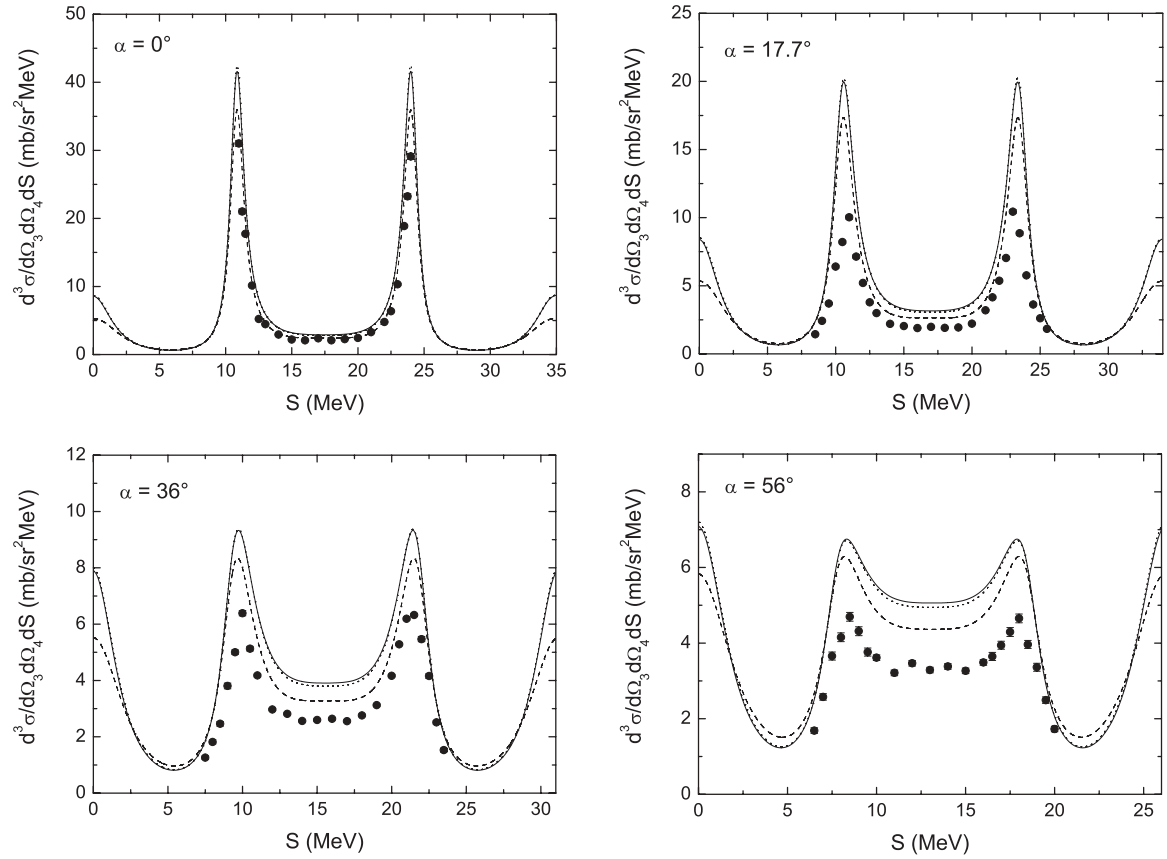

FIG. 6. Results of the SCRE breakup cross section $d^3\sigma/d\Omega_3 d\Omega_4 dS$. Experimental data are compared with the results of Faddeev calculations using the CD Bonn potential (solid), the CD Bonn potential + the Δ (dots), and the CD Bonn +Δ+ Coulomb force (dashes).

[36] in momentum-space,

$$U^{(R)}(Z) = PG_0^{-1}(Z) + PT^{(R)}(Z)G_0(Z)U^{(R)}(Z), \qquad (4)$$

$$U_0^{(R)}(Z) = (1+P)G_0^{-1}(Z) + (1+P)T^{(R)}(Z)G_0(Z)U^{(R)}(Z), \qquad (5)$$

using the standard partial-wave basis. In Eqs. (4) and (5) $G_0(Z)$ is the free resolvent, P the sum of the two cyclic permutation operators, $T^{(R)}(Z)$ the two-particle transition matrix derived from nuclear plus screened Coulomb potentials, and $U^{(R)}(Z)$ and $U_0^{(R)}(Z)$ the three-particle transition matrices for elastic and breakup scattering; their dependence on the screening radius R is notationally indicated. Finally, the renormalization procedure of Refs. [37, 38] is applied to obtain the scattering amplitudes in the unscreened limit. Further details can be found in Refs. [16, 39, 40]. The present results are well converged with respect to screening and with respect to the partial-wave expansion.

C. Chiral effective-field approach

We have also performed calculations within the chiral effective field theory (EFT) framework. This approach is based upon the approximate and spontaneously broken chiral symmetry of quantum chromodynamics. In the pion and single-nucleon sectors, it allows the S-matrix elements to be determined via the chiral expansion, i.e., the perturbative expansion in powers of the low external momenta and about the chiral limit; see e.g., Refs. [41–43]. In the case of few nucleons, this method needs to be modified to account for the nonperturbative phenomena that are, e.g., responsible for the appearance of the shallow bound states. In the present work we follow the approach suggested by Weinberg in the early 1990's [44]. In this scheme, one applies the chiral expansion to derive nuclear forces from the most general effective Lagrangian, which are then used as input in few-body calculations; see Ref. [45] and references therein. The most advanced studies of the two-nucleon system in this framework have been carried out in Refs. [46,47], where the NN forces were applied up to next-to-next-to-next-to-leading order (NNNLO) in the chiral expansion. In the three- and more-nucleon sectors, the calculations have so far been performed up to NNLO [48, 49]. While the four-nucleon force at NNNLO has already been worked out [50], the derivation of the corresponding three-nucleon forces is yet in progress. In the present study, we, therefore, restrict ourselves to NNLO and perform the calculations by using the latest generation of the chiral NN forces based on the spectral-function regularization [45, 51, 52]. Notice that while in our earlier studies [48, 49] only np forces were worked out, we now also incorporate the leading isospin-breaking effects. We further emphasize that in contrast to our previous work [53], where incomplete results at NNLO and NNNLO were presented, we are now able to perform

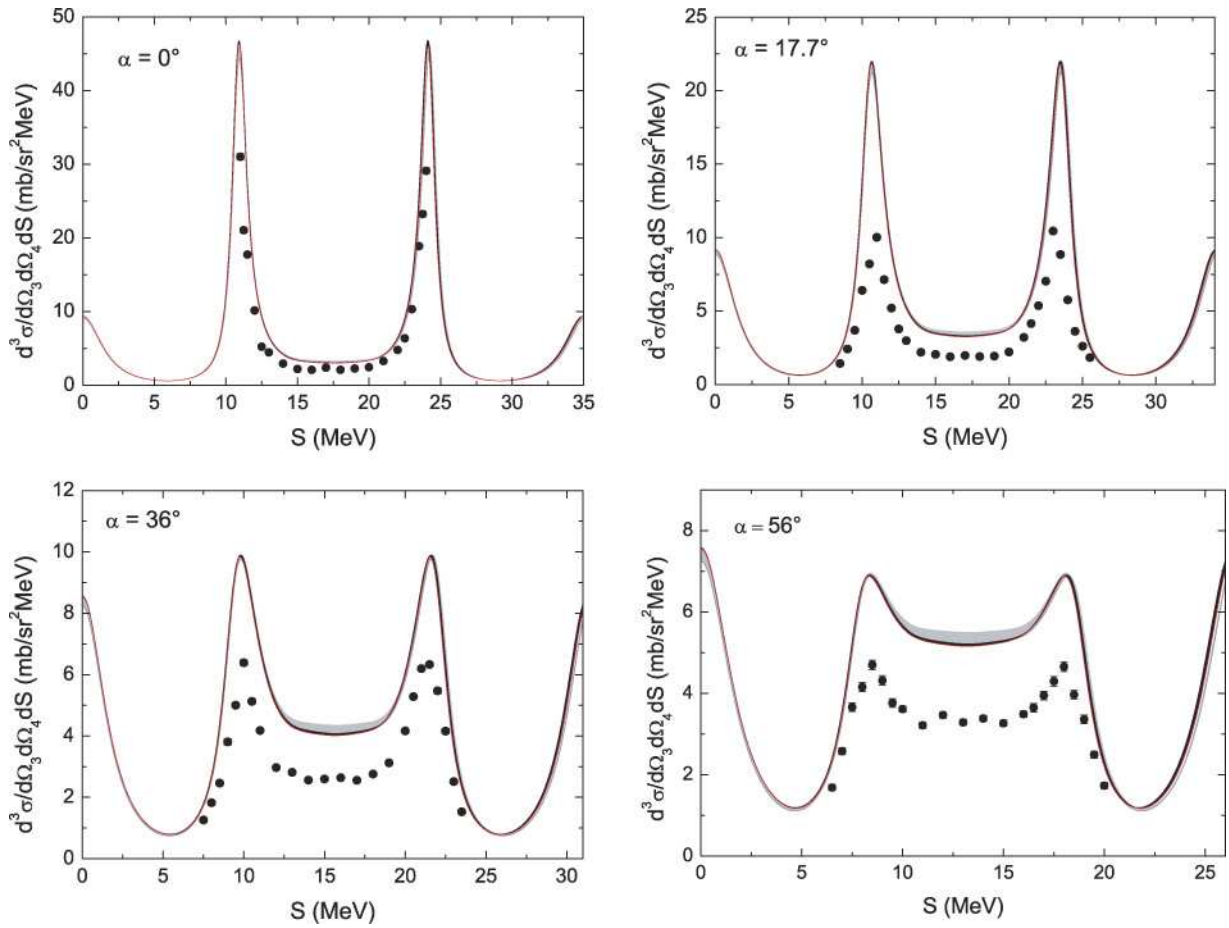

FIG. 7. (Color online) Results of the SCRE breakup cross section $d^3\sigma/d\Omega_3 d\Omega_4 dS$. Experimental data are compared with the results of calculations in the framework of the chiral EFT at NLO (gray band) and NNLO (black). The bands result from the cutoff variation; see Ref. [45] for more details.

the complete NNLO calculation including the corresponding chiral $3NF$. Finally, we refrain from giving the incomplete NNNLO results in the present study.

III. EXPERIMENT

The measurements were performed at the Cologne FN tandem Van de Graaff accelerator facility. The purely tensor-polarized deuterons were produced by the Cologne Lambshift source LASCO, equipped with a newly designed spin filter [54] with an improved figure of merit $P_{yy}^2 \times I$, and accelerated to a laboratory energy of 19.0 MeV. The beam with typical currents of 90 nA (on target) was focused into a beam spot of 2 mm diameter inside an Ortec 2800 scattering chamber. The pure tensor polarization P_{yy} was achieved by selecting the $m_I = 0$ metastable $(2S_{1/2})$ deuteron substate in the spinfilter on LASCO and precessing the polarization in a subsequent Wien filter into the vertical (laboratory) y axis. The beam polarization was measured by a five-detector polarimeter, based on the $^3\mathrm{He}(\vec{d},p)^4\mathrm{He}$ reaction, mounted inside the Faraday cup behind the scattering chamber. P_{yy} values of -1.37 (about 69% of the theoretical value) were achieved. Figure 1 shows the experimental setup including the polarimeter.

The target foils used in our measurement consisted of solid polyethylene $(CH_2)_n$ with a thickness of 600–700 μg/cm^2 and a carbon backing layer of $\sim 40-50$ μg/cm^2 on each side and were mounted in a triple target holder. Rotation of the targets with about 700 rpm provided for a greatly (up to a factor 10) increased target lifetime.

For the detection of protons of the dp breakup reaction and the elastic and inelastic deuteron scattering from carbon and ^{1}H, we used 2000-μm-thick room-temperature silicon surface barrier detectors with an energy resolution of better than $\sim$50 keV (FWHM). SCRE situations are characterized by the requirement that all three outgoing particles have equal absolute momenta and be emitted under 120° relative to one another, thus forming a planar star. In our case the two protons are emitted symmetrically to a plane formed by the beam (z axis) and the vertical y axis (the alignment direction of the beam polarization). The orientation of this plane is determined by the angle α between the negative z axis and the momentum vector of the outgoing neutron. Four SCRE situations are measured simultaneously, including a coplanar star situation ($\alpha = 0°$).

The detectors were positioned with an accuracy of $\pm 0.1°$ and ± 1 mm in the scattering chamber in a left-right symmetric arrangement for four coincidences. Table I shows the scattering angles for all coincidence detectors.

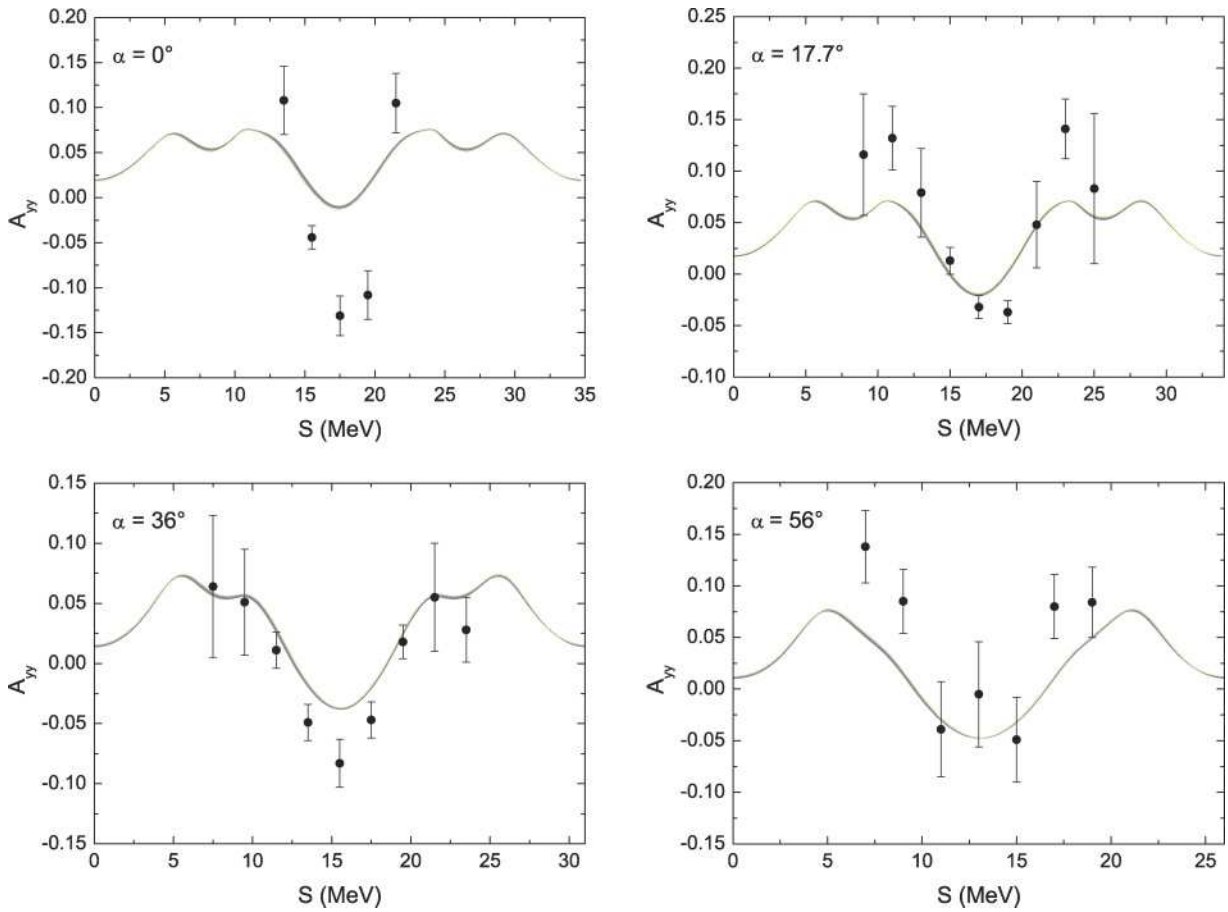

FIG. 8. (Color online) Same as in Fig. 4 for the breakup tensor analyzing power A_{yy}.

Two additional detectors at laboratory angles of $\theta = 28.5^{\circ}, \phi = 0^{\circ}, 180^{\circ}$ served as monitors for the absolute normalization of the breakup cross section. Each detector had a total counting rate of less than 8 kHz and therefore no significant dead time or pileup effects occurred. The signals from all detectors were processed simultaneously by our new coincidence electronics and recorded in list mode on magnetic tape.

The main features of this new setup are the use of QDCs (charge-to-digital converters) and an MLU (memory look-up unit), which allows free programming of arbitrary coincidences between as many as 16 detectors in very short time.

TABLE I. SCRE angle α and corresponding laboratory angles of coincidence and monitor detectors (deg), detector distances from target (mm), and solid angles (msr).

α	$\theta_{3,4}$	ϕ_3	ϕ_4	$r_{3,4}$	$\Delta\Omega_{3,4}$
0.00	21.01	0.00	180.00	291.2	0.588
17.70	21.51	9.96	170.04	290.1	0.597
36.00	22.95	18.75	161.25	290.1	0.597
56.00	25.26	25.58	154.42	291.2	0.588
Monitor	28.5	0.00	180.00	263.0	0.045

Each coincidence event consisted of at least three logical status words followed by data words containing the kinematical configuration, the energies, and the time-of-flight differences of the particles detected. From the eight or more list-mode words, energy and time-difference data triplets were created. To control the experiment online, the software package PAW (Physics Analyzing Workstation) [55] was used. The coincidence events were checked by incrementing and displaying two-dimensional energy spectra, background-corrected S-curve projections, and distance-parameter spectra.

IV. DATA ANALYSIS

The coincidence events were stored as triplets (E_3, E_4, Δt), event by event, on magnetic tape together with a status word. At vanishing angular and energy resolutions in a kinematically complete measurement the breakup events appear on ideal point-geometry kinematical loci in the E_3, E_4 plane. The measured events scatter around these ideal (point-geometry) kinematical loci mainly because of finite detector apertures.

For the projection of the breakup events onto the kinematical curve (S curve) we assumed a two-dimensional Gaussian distribution of the data around this curve. Therefore the correct projection of a true (E_3, E_4) event was done by assigning it the proper location on the point-geometry kinematical curve

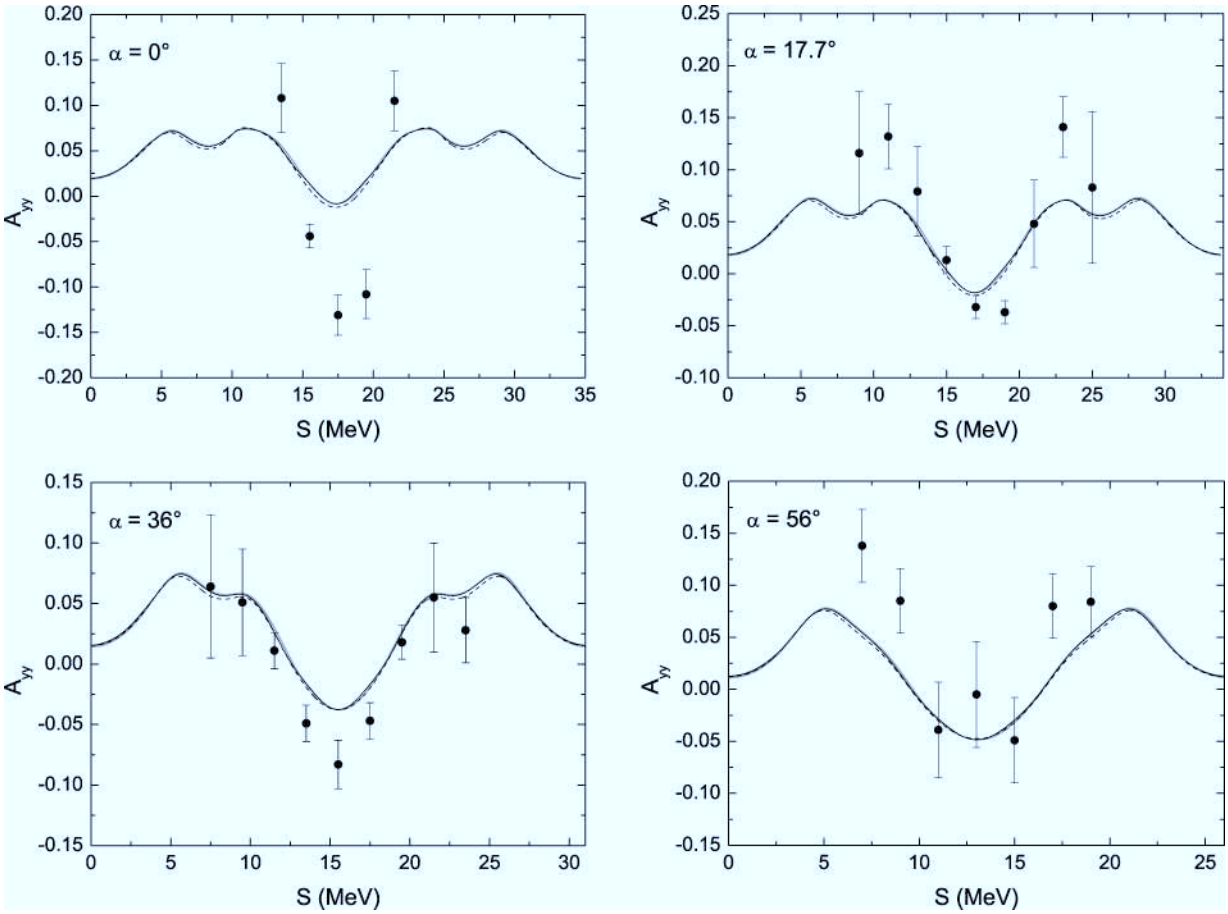

FIG. 9. Same as in Fig. 5 for the breakup tensor analyzing power A_{yy}.

by using reference matrices. For every event in the calibrated E_3–E_4 plane the reference matrices contain the numerically calculated information about the shortest distance to the S curve.

A. Time-difference spectra and background subtraction

Shown in Fig. 2 is a typical E_3–E_4 event matrix with true coincident events along the kinematical locus and background from accidental coincidences. This background consisted mainly of random coincidences due to elastic scattering and reactions with the target nuclei ^{2}H and ^{12}C and truly random coincidences from various sources. The background-correction procedure is based on methods similar to those described in [14, 56, 57] and is therefore summarized briefly. First, time-of-flight differences are calculated from the known distances of the detectors to the target and under the assumption that the particle masses were those of the detected nucleons of the *pd* breakup. Thus a linear relation between the calculated and measured time-of-flight differences is expected. When two-dimensional time-difference matrices are built by sorting the events according to their calculated time-of-flight differences and the directly measured time-of-flight differences (Fig. 3), the true breakup events therefore produce a straight ridge above the uniformly distributed random coincidence events. The smaller enclosed region C(tr+r) on the right in Fig. 3 encompasses this peak but also contains a contribution from random coincidences that has to be subtracted. The larger polygon C(r) on the left contains only random events. It has the area of the "true + random" polygon C(tr+r), suitably enlarged by a factor V in the Δt_{exp} direction (with V as large as possible). The error from the random-background subtraction enters only with this reduction factor V.

B. Distance-parameter spectra

To subtract the accidental background properly, all events in the two time-difference windows at a given distance from the kinematical locus are summed up along the kinematical curve. The "true" distance-parameter spectrum is obtained by subtracting the "accidental" from the "true+accidental" spectrum. Only the remaining true events are used for projections onto the S curve.

C. *S*-curve projection

Thus, after application of our projection procedure to both regions C(tr+r) and C(r), the number of true *pd* breakup events is given by

$$N_{\mathrm{tr}}(\Delta S_\mu) = N_{\mathrm{tr+r}}(\Delta S_\mu) - \frac{1}{V} N_{\mathrm{r}}(\Delta S_\mu) \qquad (6)$$

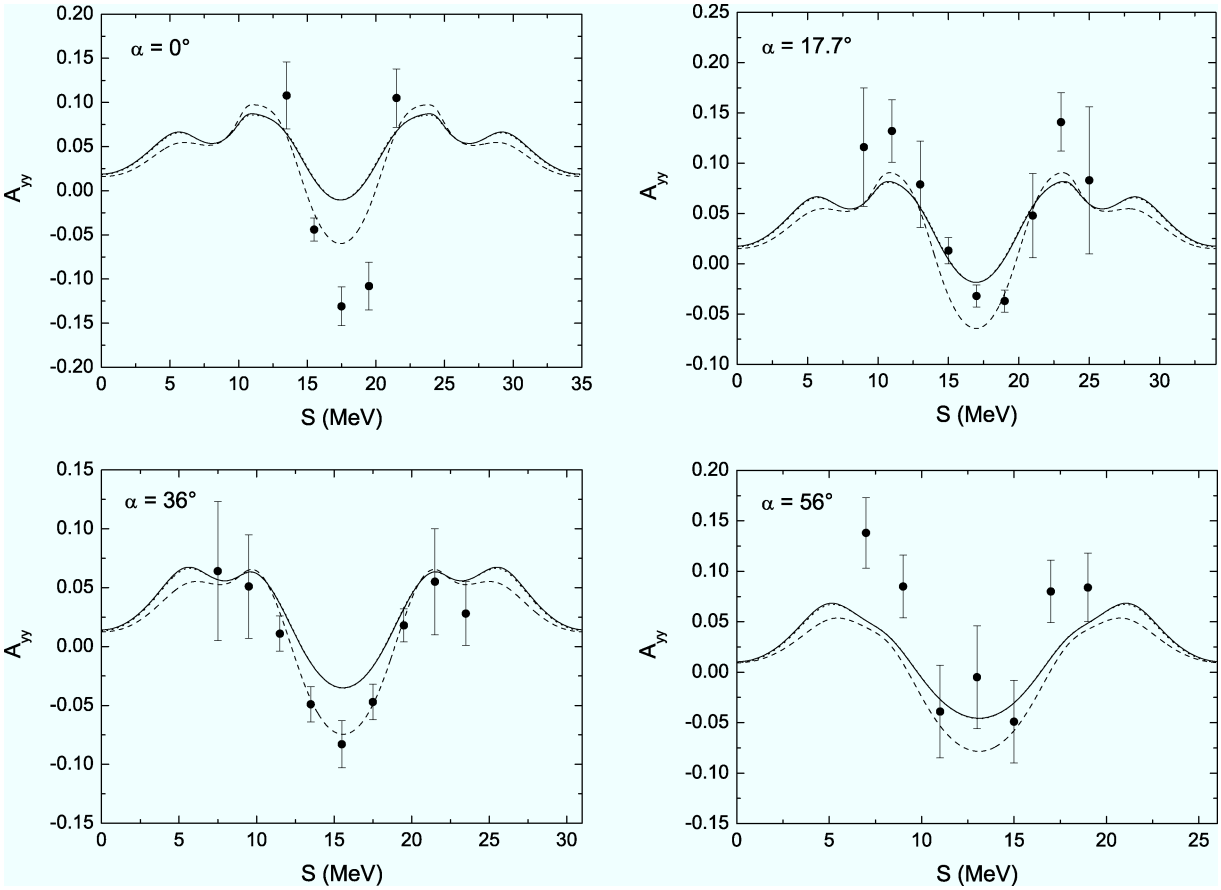

FIG. 10. Same as in Fig. 6 for the tensor analyzing power A_{yy}.

with a statistical error of

$$\Delta_S N_{\rm tr}(\Delta S_\mu) = \sqrt{N_{\rm tr+r}(\Delta S_\mu) + \frac{1}{V^2} N_{\rm r}(\Delta S_\mu)}, \qquad (7)$$

where ΔS_μ refers to discrete bins with this width on the S curve.

As discussed in Ref. [57], the choice of the binning width ΔS_μ is—within certain limits—somewhat arbitrary but should be governed by the criterion that narrow structures should not be distorted. Here, for the cross sections, bin widths of between 0.25 and 1.0 MeV, for the analyzing powers with their much less pronounced structure, of 2.0 MeV were chosen.

The yields of our S-curve spectra were normalized by using the relation

$$\frac{d^3\sigma}{d\Omega_3 d\Omega_4 dS} = \frac{N_{34}}{\Delta\Omega_3 \cdot \Delta\Omega_4 \cdot \Delta S_\mu} \frac{\Delta\Omega_{\rm mon}}{N_{\rm mon} \left(\frac{d\sigma}{d\Omega}\right)^{\rm lab}_{\rm mon}}, \qquad (8)$$

where $(d\sigma/d\Omega)^{\rm lab}_{\rm mon}$ denotes the differential cross section of the monitor reaction, $\Delta\Omega_{\rm mon}$ is the solid angle of the monitor detector, and $N_{\rm mon}$ is the background and dead-time corrected monitor peak intensity. N_{34} is the true (i.e., background and dead-time corrected) pd breakup intensity over an interval ΔS_μ of the arc length S. $\Delta\Omega_3$ and $\Delta\Omega_4$ are the solid angles of the coincidence detectors. The monitor reaction was ^{1}H(d,d)^{1}H, for which the elastic scattering cross section and analyzing power data have been published [58]. Of the two possible laboratory cross sections we chose the higher one, which also corresponds to the higher-energy deuteron peak with lower background. Explicitly we used the laboratory elastic scattering cross section values at 19.0 MeV and $\theta_{\rm lab} = 28.5^\circ$ calculated from c.m. cross sections of Ref. [58], which are in good agreement with the values of Ref. [59]:

$$\left(\frac{d\sigma}{d\Omega}\right)^{\rm c.m.}_{\rm mon} = (32.25 \pm 0.14)\ {\rm mb/sr}. \qquad (9)$$

The analyzing powers were calculated by taking ratios of yields from polarized over unpolarized runs for each bin at S (with width S_μ) according to

$$A_{yy}(S, \Delta S_\mu) = \frac{2}{(P_{yy})_{m_I = 0}} \left(\frac{N_{\rm pol}(S, \Delta S_\mu)}{N_{\rm unpol}(S, \Delta S_\mu)} - 1 \right). \qquad (10)$$

The errors of the results for the breakup cross section are of different origins. The main systematic error is due to the normalization cross section and the errors of the solid angles. Additionally, we have another systematic error from the projection procedure due to the distribution of the breakup events around the kinematical point-geometry loci and uncertainties of their assignment to the correct location there. Therefore we had to choose a maximum distance from the S curve within which the true breakup events were expected. We took a distance of typically 0.8 MeV.

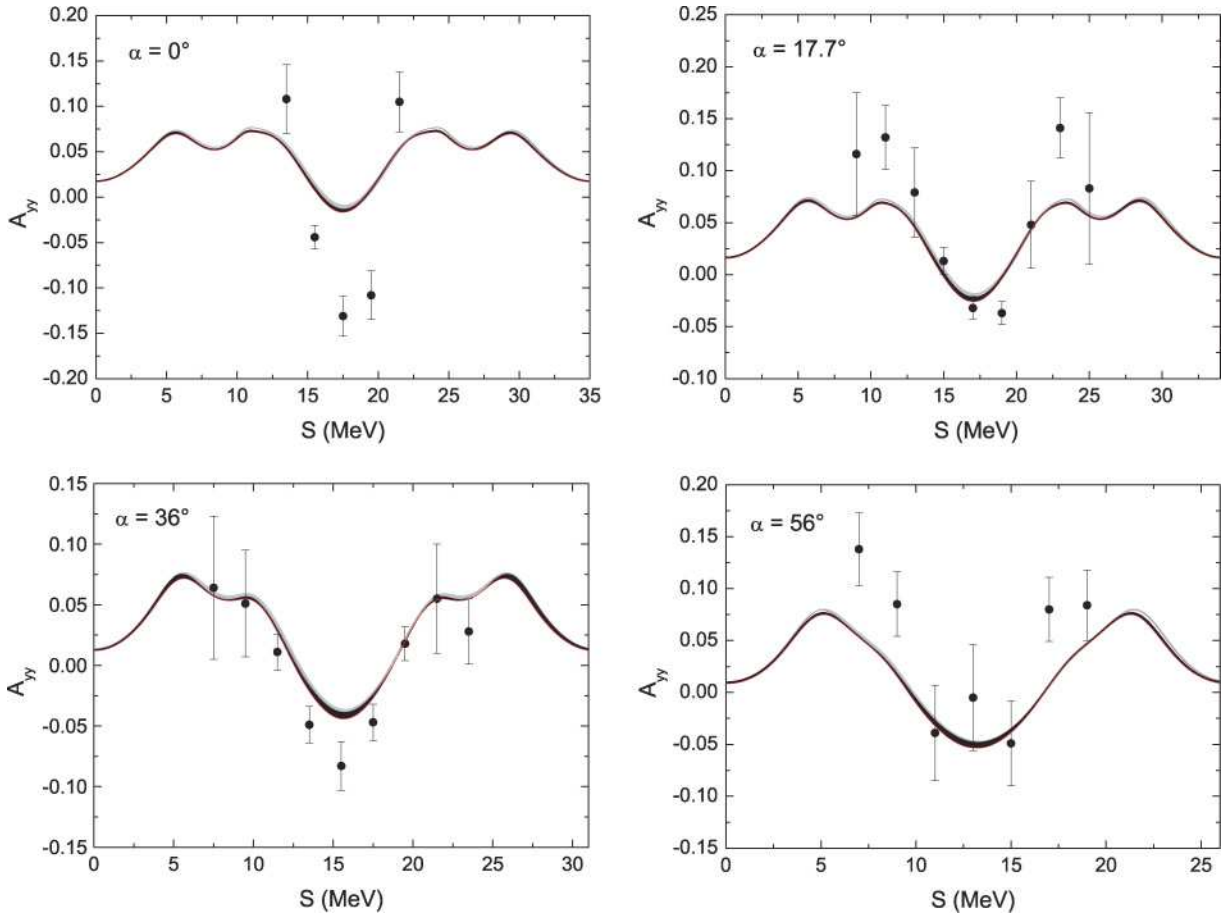

FIG. 11. (Color online) Same as in Fig. 7 for the tensor analyzing power A_{yy}.

The possible loss of breakup events due to these cuts was checked by varying the maximum distance from the S curve. For the true breakup events this loss is less than 1%. Statistical errors were assumed to originate from the absolute breakup yield and the background subtraction. These errors depend on the bin width chosen; in our case typical relative cross-section errors between 1% and 3% and typical absolute errors of the tensor analyzing powers A_{yy} of ≈0.1 resulted. The relatively large errors ΔA_{yy} despite small statistical errors result from the error propagation in Eq. (10). A previous study of the effects of averaging over the finite target-detector geometry in the case of the relatively narrow structures of the final-state interaction situation and only at the FSI peaks proper had shown that the cross section is lowered by at most 1.2%. Therefore, here the comparison is made with point-geometry calculations only.

V. RESULTS AND DISCUSSION

We compare our data with theoretical predictions from classical Faddeev calculations, using the modern high-precision NN potentials alone or combined with the present $3NF$s. Also, a comparison with chiral forces up to NNLO is made. To see the importance of effects due to the Coulomb force, we also present theoretical predictions based on CD Bonn with and without the Δ excitation and with the Δ excitation + Coulomb force included.

A. Cross sections

In Figs. 4 and 5 we present our dp breakup cross sections for the four SCRE configurations and compare them with point-geometry theoretical predictions based on modern NN potentials, alone or combined with $3NF$s. With shapes of the data quite similar to the predictions for all four SCRE geometries there is a significant overestimation (up to about 40%) of the data by the theory. The effect is even larger than what has been observed in previous investigations for the SST configuration. The different theoretical predictions based on NN forces alone are very close together, reflecting nearly on-shell equivalence of these high-precision interactions. Including the TM99' $3NF$ changes the predictions only slightly. The cross sections almost do not depend on the choice of the NN potential with which the TM99' $3NF$ is combined. Replacing the TM99' by the Urbana IX $3NF$ in the case of the AV18 potential leads to practically the same cross sections. The largest $3NF$ effects are in a region of central S values. They move the theory in the direction of the data by ≈8% at $\alpha = 0^{\circ}$. They decrease with increasing α and reach ≈5% at $\alpha = 56^{\circ}$.

Since in these calculations the Coulomb force between protons has been omitted, we show the CD Bonn and CD Bonn + Δ as well as the CD Bonn + Δ + Coulomb force predictions in Fig. 6. It is seen that inclusion of the Coulomb force moves the theory in the direction of the data. However,

only ≈30% of the discrepancy is explained in this way. The inclusion of the Δ has very little effect.

As shown in Fig. 7, the calculations in the framework of chiral EFT yield results for the cross sections very similar to the ones obtained from the conventional nuclear-force models (cf. Figs. 4, 5, and 6) and strongly overestimate the data. We further notice that the theoretical uncertainty resulting from the cutoff variation is rather small and significantly reduced at NNLO as compared with at NLO.

B. Analyzing powers A_{yy}

In the case of the tensor analyzing powers A_{yy} shown in Figs. 8 and 9 the agreement between data and theory in the three out-of plane cases is much better than for the cross sections. Only in the coplanar case ($\alpha = 0^\circ$) does a significant deviation along the kinematical locus exist. Also, here different potentials provide practically the same A_{yy} values (see Fig. 8), and inclusion of TM99' or Urbana IX $3NF$s has negligible effects (see Fig. 9). Again, combining $3NF$s with different NN potentials results in practically the same A_{yy} values. Similarily, the effect of the virtual Δ-isobar excitation is small (see Fig. 10). However, the inclusion of the Coulomb force significantly changes A_{yy}, especially in the region of the kinematical locus around the minimum of A_{yy}, thus leading to an improved description of the data, especially for $\alpha = 36^\circ$.

Similar to the case of cross sections, chiral predictions shown in Fig. 11 are very close to the results based on high-precision NN potentials. Small but visible differences may be observed for the configuration with $\alpha = 36^\circ$.

VI. SUMMARY

We present new deuteron breakup cross-section and tensor analyzing-power data for four SCRE breakup situations of the $^1\mathrm{H}(\vec{d},pp)n$ reaction. The comparison with the theoretical predictions based on different high-precision NN potentials reveals a serious overestimation of the cross section data by the theory. This overestimation is not removed when the TM99' or Urbana IX $3NF$s are included. Their effects are small. Chiral EFT results at NLO and NNLO are consistent with those based on the conventional nuclear force models and show the same deviations from the data. The uncertainty due to the cutoff variation is rather small at both orders. Also, the effects of virtual Δ-isobar excitations on the cross sections are very small. Inclusion of the Coulomb force removes some part of the discrepancy for the cross section. A similar picture exists for the tensor analyzing power A_{yy}. In the coplanar-geometry case none of the theories reproduces the data. For the out-of-plane geometries $3NF$ effects are small. The Coulomb force leads to a better agreement between data and theory, and its effect is larger than any differences between predictions of various NN and $3N$ interaction models. This indicates that rigorous theoretical studies of pd data necessitate the inclusion of the Coulomb interaction.

ACKNOWLEDGMENTS

This work was supported by the Deutsche Forschungsgemeinschaft (DFG) under grants PA 488/4-3 and PA 488/4-4. Partial financial support from the EU Integrated Infrastructure Initiative Hadron Physics Project (contract RII3-CT-2004-506078) and DFG (SFB/TR 16, "Subnuclear Structure of Matter") is gratefully acknowledged. This work was also supported by the Polish Committee for Scientific Research under grant 2P03B00825, by the U.S. Department of Energy under grants DE-FG03-00ER41132, DE-FC02-01ER41187, and DE-AC05-84ER40150 under which the Southeastern Universities Research Association (SURA) operates the Thomas Jefferson Accelerator Facility. Part of the numerical calculations was performed on the IBM Regatta p 690+ of the NIC in Jülich, Germany.

[1] W. Glöckle, H. Witała, D. Hüber, H. Kamada, and J. Golak, Phys. Rep. **274**, 107 (1996).
[2] H. Witała, D. Hüber, and W. Glöckle, Phys. Rev. C **49**, R14 (1994).
[3] A. Kievsky, M. Viviani, and S. Rosati, Phys. Rev. C **52**, R15 (1995).
[4] A. Kievsky, S. Rosati, W. Tornow, and M. Viviani, Nucl. Phys. **A607**, 402 (1996).
[5] H. Witała, W. Glöckle, D. Hüber, J. Golak, and H. Kamada, Phys. Rev. Lett. **81**, 1183 (1998).
[6] S. Nemoto, K. Chmielewski, S. Oryu, and P. U. Sauer, Phys. Rev. C **58**, 2599 (1998).
[7] M. Stephan, K. Bodek, J. Krug, W. Lübcke, S. Obermanns, H. Rühl, M. Steinke, D. Kamke, H. Witała, Th. Cornelius, and W. Glöckle, Phys. Rev. C **39**, 2133 (1989).
[8] J. Strate, K. Geißdörfer, R. Lin, W. Bielmeier, J. Cub, A. Ebneth, E. Finckh, H. Friess, G. Fuchs, K. Gebhardt, and S. Schindler, Nucl. Phys. **A501**, 51 (1989).
[9] K. Gebhardt, W. Jäger, C. Jeitner, M. Vitz, E. Finckh, T. N. Frank, Th. Januschke, W. Sandhas, and H. Haberzettl, Nucl. Phys. **A561**, 232 (1993).
[10] H. R. Setze, C. R. Howell, W. Tornow, R. T. Braun, W. Glöckle, A. H. Hussein, J. M. Lambert, G. Mertens, C. D. Roper, F. Salinas, I. Šlaus, D. E. Gonzáles Trotter, B. Vlahović, R. L. Walter, and H. Witała, Phys. Lett. **B388**, 229 (1996).
[11] Z. Zhou, A. S. Crowell, J. Deng, W. Glöckle, C. R. Howell, H. Kamada, B. Qi, R. A. Macri, X. Ruan, H. Tang, R. L. Walter, and H. Witała, Nucl. Phys. **A684**, 545c (2001).
[12] G. Rauprich, S. Lemaître, P. Niessen, K. R. Nyga, R. Reckenfelderbäumer, L. Sydow, H. Paetz gen. Schieck, H. Witała, and W. Glöckle, Nucl. Phys. **A535**, 313 (1991).
[13] R. Großmann, G. Nitzsche, H. Patberg, L. Sydow, S. Vohl, H. Paetz gen. Schieck, J. Golak, H. Witała, W. Glöckle, and D. Hüber, Nucl. Phys. **A603**, 161 (1996).
[14] H. Patberg, R. Großmann, G. Nitzsche, L. Sydow, S. Vohl, and H. Paetz gen. Schieck, Phys. Rev. C **53**, 1497 (1996).
[15] T. Ishida, T. Yagita, S. Ochi, S. Nozoe, K. Tsuruta, F. Nakamura,

H. P. g. Schieck, and K. Sagara, Mod. Phys. Lett. A **18**, 436 (2003).
[16] A. Deltuva, A. C. Fonseca, and P. U. Sauer, Phys. Rev. C **72**, 054004 (2005).
[17] W. Tornow, H. Witała, and A. Kievsky, Phys. Rev. C **57**, 555 (1998).
[18] S. A. Coon, M. D. Scadron, P. C. McNamee, B. R. Barrett, D. W. E. Blatt, and B. H. J. McKellar, Nucl. Phys. **A317**, 242 (1979).
[19] S. A. Coon and W. Glöckle, Phys. Rev. C **23**, 1790 (1981).
[20] A. Nogga, D. Hüber, H. Kamada, and W. Glöckle, Phys. Lett. **B409**, 19 (1997).
[21] H. Witała, W. Glöckle, J. Golak, D. Hüber, H. Kamada, W. Tornow, E. Stephenson, and D. A. Low, Phys. Rev. C **52**, 2906 (1995).
[22] L. M. Qin, W. Boeglin, D. Fritschi, J. Götz, J. Jourdan, G. Masson, S. Robinson, I. Sick, P. Trueb, M. Tucillo, B. Zihlmann, H. Witała, J. Golak, W. Glöckle, and D. Hüber, Nucl. Phys. **A587**, 252 (1995).
[23] H. Paetz gen. Schieck, H. Witała, J. Golak, J. Kuroś, and R. Skibiński, Few-Body Systems **30**, 81 (2001).
[24] R. B. Wiringa, V. G. J. Stoks, and R. Schiavilla, Phys. Rev. C **51**, 38 (1995).
[25] R. Machleidt, F. Samarucca, and Y. Song, Phys. Rev. C **53**, R1483 (1996).
[26] V. G. J. Stoks, R. A. M. Klomp, C. P. F. Terheggen, and J. J. de Swart, Phys. Rev. C **49**, 2950 (1994).
[27] S. Pudliner, V. R. Pandharipande, J. Carlson, S. C. Pieper, and R. B. Wiringa, Phys. Rev. C **56**, 1720 (1997).
[28] H. Witała, Th. Cornelius, and W. Glöckle, Few-Body Syst. **3**, 123 (1988).
[29] W. Glöckle, *The Quantum Mechanical Few-Body Problem* (Springer-Verlag, Berlin, 1983).
[30] D. Hüber, H. Witała, and W. Glöckle, Few-Body Syst. **14**, 171 (1993).
[31] D. Hüber, H. Kamada, H. Witała, and W. Glöckle, Acta. Phys. Pol. B **28**, 1677 (1997).
[32] H. Witała, W. Glöckle, and H. Kamada, Phys. Rev. C **43**, 1619 (1991).
[33] J. Friar, D. Hüber, and U. van Kolck, Phys. Rev. C **59**, 53 (1999).
[34] S. A. Coon and H. K. Han, Few-Body Syst. **30**, 131 (2001).
[35] A. Deltuva, R. Machleidt, and P. U. Sauer, Phys. Rev. C **68**, 024005 (2003).
[36] E. O. Alt, P. Grassberger, and W. Sandhas, Nucl. Phys. **B2**, 167 (1967).
[37] J. R. Taylor, Nuovo Cimento B **23**, 313 (1974); M. D. Semon and J. R. Taylor, Nuovo Cimento A **26**, 48 (1975).
[38] E. O. Alt, W. Sandhas, and H. Ziegelmann, Phys. Rev. C **17**, 1981 (1978); E. O. Alt and W. Sandhas, *ibid*. **21**, 1733 (1980).
[39] A. Deltuva, K. Chmielewski, and P. U. Sauer, Phys. Rev. C **67**, 034001 (2003).
[40] A. Deltuva, A. C. Fonseca, and P. U. Sauer, Phys. Rev. C **71**, 054005 (2005).
[41] V. Bernard, N. Kaiser, and U.-G. Meißner, Int. J. Mod. Phys. E **4**, 193 (1995).
[42] A. Pich, Rep. Prog. Phys. **58**, 563 (1995).
[43] J. Gasser, Lect. Notes Phys. **629**, 1 (2004).
[44] S. Weinberg, Phys. Lett. **B251**, 288 (1990); Nucl. Phys. **B363**, 3 (1991).
[45] E. Epelbaum, Prog. Part. Nucl. Phys. (in press).
[46] D. R. Entem and R. Machleidt, Phys. Rev. C **68**, 041001 (2003).
[47] E. Epelbaum, W. Glöckle, and U.-G. Meißner, Nucl. Phys. **A747**, 362 (2005).
[48] E. Epelbaum, A. Nogga, W. Glöckle, H. Kamada, U.-G. Meißner, and H. Witała, Phys. Rev. C **66**, 064001 (2002).
[49] E. Epelbaum, H. Kamada, A. Nogga, H. Witała, W. Glöckle, and U.-G. Meißner, Phys. Rev. Lett. **86**, 4787 (2001).
[50] E. Epelbaum, arXiv.org:nucl-th/0511025.
[51] E. Epelbaum, W. Glöckle, and U.-G. Meißner, Eur. Phys. J. A **19**, 125 (2004).
[52] E. Epelbaum, W. Glöckle, and U.-G. Meißner, Eur. Phys. J. A **19**, 401 (2004).
[53] C. Düweke, R. Emmerich, A. Imig, J. Ley, G. Tenckhoff, H. Paetz gen. Schieck, J. Golak, H. Witała, E. Epelbaum, W. Glöckle, and A. Nogga, Phys. Rev. C **71**, 054003 (2005).
[54] J. L. McKibben, G. P. Lawrence, and G. G. Ohlsen, Phys. Rev. Lett. **20**, 1180 (1968).
[55] CERN Program Library Long Writeup **Q121**, PAW, 1995.
[56] D. Gola, W. Bretfeld, W. Burgmer, H. Eichner, Ch. Heinrich, H. J. Helten, H. Kretzer, K. Prescher, H. Oswald, W. Schnorrenberg, and H. Paetz gen. Schieck, Phys. Rev. C **27**, 1394 (1983).
[57] M. Przyborowski, M. Eggert, R. Engels, M. Menzel, L. Sydow, H. Paetz gen. Schieck, H. Witała, J. Golak, J. Kuroś, and W. Glöckle, Phys. Rev. C **60**, 064004 (1999).
[58] W. Grüebler, V. König, P. A. Schmelzbach, F. Sperisen, B. Jenny, R. E. White, F. Seiler, and H. W. Roser, Nucl. Phys. **A398**, 445 (1983); W. Grüebler (private communication, 1983).
[59] K. Sagara, H. Oguri, S. Shimizu, K. Maeda, H. Nakamura, T. Nakashima, and S. Morinobu, Phys. Rev. C **50**, 576 (1994).